NASA

Technical Memorandum 80717

(NASA-TM-80717) SYNOPTIC OBSERVATIONS OF JUPITER'S RADIO EMISSIONS: AVERAGE STATISTICAL PROPERTIES OBSERVED BY VOYAGER (NASA) 43 p HC A03/MF A01 CSCL 03B

N80-28285

Unclas
G3/91 25209

Synoptic Observations of Jupiter's Radio Emissions: Average Statistical Properties Observed by Voyager

J. K. Alexander, T. D. Carr, J. R. Thieman, J. J. Schauble, and A. C. Riddle

JUNE 1980

National Aeronautics and Space Administration

Goddard Space Flight Center
Greenbelt, Maryland 20771

SYNOPTIC OBSERVATIONS OF JUPITER'S RADIO EMISSIONS: AVERAGE STATISTICAL PROPERTIES OBSERVED BY VOYAGER

J. K. Alexander,[1] T. D. Carr,[2] J. R. Thieman,[3]
J. J. Schauble,[4] and A. C. Riddle[5]

1. Laboratory for Extraterrestrial Physics, NASA/Goddard Space Flight Center, Greenbelt, Maryland 20771
2. Department of Astronomy, University of Florida, Gainesville, FL 32608
3. Space Systems Analysis Division, ORI, Inc., Silver Spring, MD 20910
4. University of Florida Graduate Center, Eglin Air Force Base, FL 32542
5. CIRES, University of Colorado, Boulder, CO 80309

SUBMITTED TO: Journal of Geophysical Research

ABSTRACT

Observations of Jupiter's low frequency radio emissions collected over one-month intervals before and after each Voyager encounter have been analyzed to provide a synoptic view of the average statistical properties of the emissions. Compilations of occurrence probability, average power flux density and average sense of circular polarization are presented as a function of central meridian longitude, phase of Io, and frequency. The results are compared with ground-based observations. The necessary geometrical conditions and preferred polarization sense for Io-related decametric emission observed by Voyager from above both the dayside and nightside hemispheres are found to be essentially the same as are obs rved in Earth-based studies. On the other hand, there is a clear local time dependence in the Io-independent decametric emission. This emission is prevalent at longitudes above 200° when observed from over the dayside hemisphere but is dominant at longitudes below 200° when observed from over the post-midnight sector. Decametric emission which comprises the dynamic spectral lesser arcs near 10 MHz displays a distinct, bimodal polarization pattern that is predominantly in the left-hand sense at longitudes below 150° and in the right-hand sense at longitudes above 150°. The central meridian longitude distributions of occurrence probability and average flux density at hectometric wavelengths appear to depend significantly on both the observer's latitude and local time. Io appears to have an influence on average flux density of the emission down to below 2 MHz. The average power flux density spectrum of Jupiter's emission has a broad peak near 9 MHz. Integration of the average spectrum over all frequencies gives a total radiated power for an isotropic source of 4×10^{11} W.

I. INTRODUCTION

Ever since the discovery of Jupiter's low frequency radio emissions a quarter-century ago, a number of observers have systematically monitored the planetary radio source and have carefully compiled statistical descriptions of the average properties of the sporadic decameter-wave radiation. These studies have lead to a comprehensive description of such morphological properties of the emissions as the variation in level of activity as a function of frequency, central meridian longitude of Jupiter, phase of Io,

jovicentric latitude of Earth, etc. And in turn, these morphological summaries have provided the basis for many of our initial models of the nature of the Jovian magnetic field, of the role of Io in the coupling of Jupiter's ionosphere and magnetosphere, and of course, of the nature of the radio source itself.

The Voyager Planetary Radio Astronomy (PRA) measurements, although collected over a relatively short span of time, are capable of complementing and extending the wealth of earlier ground-based and near-earth satellite observations to provide the first description of the radio emission morphology over the full low frequency spectrum (20 kHz–40 MHz). In this paper we present a statistical description of the variations in the occurrence probability, power flux density and sense of circular polarization of the radio emissions as they were observed from the unique perspective afforded by Voyager.

We take advantage of three special aspects of the Voyager mission. First, we can survey the complete spectrum between the high frequency limit of the decametric emissions near 40 MHz and the low frequency limit imposed by Jovian propagation cut-offs below 0.1 MHz. Ground-based observations have generally been restricted to frequencies above the critical frequency of the terrestrial ionosphere (typically 5–10 MHz), and these have been supplemented by a few observations down to about 0.5 MHz from Earth-orbit with modest sensivity and frequency resolution. Second, the very close proximity of Voyager to Jupiter provides an improvement of several orders of magnitude in the sensitivity of our survey compared to what is typical from Earth. For example, the measurements taken at ranges of approximately 50 to 400 R_J and used in this paper have a sensitivity threshold that is 9 to 27 dB lower than for a five-element Yagi antenna of the type most often used in ground-based synoptic monitoring programs. Third, the post-encounter Voyager data provide a view of the radio emissions from above the night hemisphere of Jupiter--a perspective that is impossible to obtain from Earth.

In order to study variations in the properties of Jupiter emissions that may result from a changing observer-Jupiter-sun angle we have analyzed one-month intervals both before and after each Voyager encounter. The general

circumstances of that survey are summarized in Figure 1. The days immediately preceding and following closest approach were not included because ghost image effects due to intense, saturation level signals in the high-frequency band of the PRA receiver sometimes confuse the unambiguous identification of high frequency decameter-wave activity and because the wide range of spacecraft-Jupiter-sun angles which occurred during this period were not sampled for long enough intervals to yield statistically significant results. Note that the spacecraft approached Jupiter from above the pre-noon sector at local times (09.5 and 11.0 hr) that do not quite overlap the range covered by terrestrial observations (11.3-12.7 hr). After encounter both spacecraft are over the post-midnight quadrant at approximately 03 hr local time (Voyager-2) and 04 hr local time (Voyager-1). The two spacecraft approached Jupiter from jovigraphic latitudes of approximately $+3^{\circ}$ (Voyager-1) and $+7^{\circ}$ (Voyager-2), and both followed post-encounter trajectories at latitudes near $+5^{\circ}$. For the large body of terrestrial studies, only a region bounded by local times within $\pm 11^{\circ}$ of the noon meridian and latitudes between -3.3° and $+3.3^{\circ}$ have been sampled.

It is well known that Jupiter emission varies with small changes in jovigraphic latitude [Carr and Desch, 1976; Alexander et al., 1979], but no unambiguous local time effects have been observed in the very limited angular range covered by pre-Voyager data. A local time dependence has been discovered in the earth's kilometer-wavelength radiation [Gurnett, 1974], and by analogy a similar effect might be anticipated for Jupiter. This report presents new data which reveal a significant local time and/or latitude dependence of the emission in several wavelength bands.

In the next section we present a description of the variation of occurrence probability as a function of frequency, System III central meridian longitude (CML) and phase of Io, and we call attention to changes in those patterns that occurred after each Voyager closest approach. In section III, we show how CML profiles of average flux density evolve as a function of frequency, latitude and local time, and we examine the frequency range over which evidence for Io-control can be tracked. Section IV is devoted to an overview of the variations in measured sense of polarization of the radio waves as a function of frequency and longitude. In section V we present

Voyager-2 measurements of the average power flux density spectrum over the full PRA frequency range. Finally, in section VI we summarize our major conclusions from this study and comment on some of their possible implications and limitations.

II. OCCURRENCE PROBABILITY VARIATIONS

The usual mode of display of the PRA data is the dynamic spectrum such as displayed in Boischot et al. [this issue]. Each of these spectra depend on the instantaneous properties of the magnetospheric environment in which the radio emission was generated. It is difficult to distinguish short-lived phenomena from repeatable characteristics in individual dynamic spectra since they sometimes differ significantly from each other even after only one rotation of the planet. A superposition of many spectra averages out the short-term variations and allows the underlying stable properties to be recognized. Since the principal features usually recur with the Jovian rotational period the spectra must be aligned in longitude for long-lived features to reinforce each other.

Figure 2 presents the results of the superposition of one-month spans of data from before and after each Jupiter encounter. The colors are indicative of the probability of occurrence of radiation at a particular longitude and frequency. The occurrence probability is computed as the number of activity counts divided by the number of observing counts for each frequency and each degree of CML. An activity count is registered when the activity exceeds the background level by a minimum of 1 dB. Thus, the stronger emissions are weighted equally with weaker events. The background is separately determined for each rotation. The horizontal bands that extend across all longitudes at certain discrete frequencies are due to nearly continuous interference generated by other spacecraft electronics subsystems. More noticeable are the vertical bands of interference at frequencies above 5 MHz for both spacecraft before encounter. These represent noise from a long-term periodic observing schedule by the imaging experiment. The period was approximately 2 hours and was synchronized with the Jovian rotational period so that the interference reinforces itself and appears with high probability at 72-degree intervals.

The frequency axes for Figure 2 are split into a low-frequency band of 70 channels from 1.2 kHz to 1.3 MHz spaced at 19 kHz intervals and a high-frequency band of 128 frequency channels extending from 1.5 MHz to 40 MHz in 307 kHz intervals. The low band is more sensitive and displays a clearly higher level of overall occurrence probability so that there is an abrupt discontinuity in the occurrence probability profile at 1.3 MHz. (For a more complete description of the PRA instrument, see Boischot et al. [this issue.])

Three components of Jupiter's radio spectrum are evident in Figure 2--radiation at decameter-wavelengths (DAM), hectometer-wavelengths (HOM), and kilometer wavelengths (KOM). DAM spans the frequencies of 3-40 MHz but only the activity in the range below 30 MHz shows up in the figure. This is due to the combined effect of the decreasing power of the emission with increasing frequency and the increasing dependence of activity at higher frequencies on the phase of Io. For the lower frequencies in the DAM range, the major feature is a nearly continuous band of radiation between approximately 5 and 15 MHz and extending across all longitudes except for a gap near 120°. This radiation corresponds to the nearly continuous 9 and 10 MHz radiation previously observed from the earth [Dulk and Clark, 1966]. By examining individual dynamic spectra in this band we find that it is made up primarily of the "lesser arcs" described by Boischot et al. [this issue].

When we compare occurrence probability levels at frequencies above about 15 MHz before and after each encounter, we find a relatively higher activity level at longitudes above 200° before encounter but more activity below 200° after encounter. A post-encounter enhancement of the decametric feature that drifts from about 25 MHz near 150° down to $\sim$ 10 MHz by 190° is especially clear. This feature probably corresponds to the weak Io-independent B source recorded in Earth-based surveys [Bozyan and Douglas, 1975] and is formed by the Io-independent vertex early family of dynamic spectral arcs described by Leblanc and Daigne [this issue]. Notice also that after encounter the occurrence probabilities in the band centered near 10 MHz increase significantly at high longitudes.

We compare DAM longitude profiles obtained from the Voyager measurements with ground-based data in the same frequency range in Figure 3. Here we have

plotted histograms of occurrence probability as a function of CML for ground-based observations at 22 MHz (taken from the compilation by Thieman [1979]) and for those Voyager DAM great arc emission events that extended to frequencies $\geq$ 20 MHz. The observations used to prepare the top histogram were collected during the 1976 apparition when the Jovigrapahic latitude of Earth was near its maximum value and was comparable to the Jovigraphic latitude of V1 before encounter. We find the ground observations and the Voyager pre-encounter results to be very similar. The absolute occurrence probabilities are higher for the Voyagers than for the ground observations due to the closer proximity of the spacecraft to Jupiter, and the higher occurrence probabilities for Voyager-2 (V2) compared to Voyager-1 (V1) are primarily a consequence of lower spacecraft background interference levels on V2 (by about 2 dB). The difference in observer-Jupiter-sun angle of $\sim 30^{\circ}$ between the ground-based data and V2 pre-encounter data does not appear to produce any large differences in the longitude histrograms. On the other hand, we see a complete reversal in the relative amplitudes of the early and late longitude occurrence probability maxima in the post-encounter data sets. When viewed from above the dayside hemisphere, the highest level of DAM activity at frequencies $\geq$ 20 MHz is in the 250°-280° longitude range, but when Jupiter is viewed from above the nighttime hemisphere that peak becomes secondary to the peak at 150° to 170°.

In the HOM radiation band (corresponding to frequencies between about 100 kHz and 3 MHz) we see in Figure 2 a relatively high level of activity in the longitude range from about 260° through 360° to 140° and a 100° wide low activity gap centered near 200° longitude. (The radiation appearing near 200° is the KOM component to be discussed shortly.) The overall variations of HOM occurrence probability as a function of CML show some systematic changes with spacecraft Jovicentric latitude. For example, the low occurrence probability gap is widest for V2 before encounter (latitude $\sim 7^{\circ}$, see Figure 1) and narrowest for V1 before encounter (latitude $\sim 3^{\circ}$); after encounter the width of the gap is the same for both spacecraft (latitude $\sim 5^{\circ}$) and is intermediate to the pre-encounter values. A secondary occurrence probability minimum can be found at longitudes near 30° in the V1 pre-encounter data and in both post-encounter plots but not in the V2 pre-encounter display corresponding to the highest observing latitude. These patterns are all consistent with the

latitudinal beaming model of Alexander et al. [1979] in which the HOM radiation escapes into a thin, curved sheet that is tipped a few degrees northward of the magnetic equatorial "plane" in the inner magnetosphere.

There is evidence in Figure 2 for several repeatable dynamic spectral features or "lanes" in the HOM band. Such repeatable features at HOM wavelengths were first described by Kaiser et al. [1979] and Lecacheux et al. [1980]. Lane events are defined as lower probability gaps which cut through the high probability areas as linearly increasing or decreasing functions of frequency. These are especially evident in the V2 panels of Figure 2. The lane event which occurs most often begins at a frequency of approximately 750 kHz and a longitude of 260° and ends at a frequency around 1.3 MHz near the longitude of 330°. A second lane structure begins around 1.3 MHz and 100° longitude and drifts to 750 kHz at approximately 140°.

After encounter both Voyagers show an abrupt change in occurrence probability along an edge starting at 1.3 MHz at 340° and extending downward to 500 kHz between 20° and 30°. Before encounter this feature is not apparent. The similarity of the slopes in this edge and the edge associated with the lane events suggests that they may be related. We will discuss the lane events further in the polarization section.

Finally, the typical tapered-event nature of broadband kilometric radiation (bKOM) (Desch and Kaiser [1980]) is obvious in the V2 before-encounter panel of Figure 2. Tapered events can reach a maximum frequency as high as 1 MHz and the lower limits are often tens of kilohertz. The maximum frequency for an event is usually reached at a longitude of 200°. This type of event was also observed by V1 before encounter although there was a smaller occurrence probability, and consequently the bKOM does not appear as prominent in that panel of Figure 2. After encounter the central portion of the tapered event is missing and only two fragments of the original tapered event remain, one centered at 150° and a broader, less-obvious region centered at 240°. That this is true for both spacecraft after encounter lends credence to the argument that this bifurcation is a local time effect as proposed by Desch and Kaiser [1980]. Notice that both the HOM radiation and the KOM radiation appear to extend to slightly lower frequencies after encounter.

One of the most remarkable aspects of the morphology of Jupiter's decametric radiation, especially at frequencies above about 18 MHz, is the strong dependence on the phase of Io. (We use the term "Io phase" here as short hand to denote the angular departure of Io from the observer-Jupiter line measured in the direction of Io's orbital motion from 0° when Io is situated on the opposite side of the planet from the observer. For observations from Earth, this angle is known as "the departure from superior geocentric conjunction".) In order to get an overview of the Io modulation effects in the Voyager data at decametric wavelengths we have cataloged all events observed within one month of each encounter that extended to frequencies equal to or above 20 MHz during the event. By an "event" we mean a period of decametric emission typically lasting from one-half hour to several hours and consisting of an ensemble of great arcs having the same sense of curvature and similar dynamic spectral shapes (e.g., see Figure 3 of Boischot et al. [this issue]).

The locations in CML and Io phase for those decametric events that were observed to reach peak frequencies at or above 20 MHz are plotted in Figure 4. Those events which extended to peak frequencies of 30 MHz or higher are indicated by the heavy lines. The tendency for more activity to be observed by V2 than V1 is primarily a consequence of the lower interference levels on V2.

Concentrating on the data taken before encounter (left-hand panels of Figure 4), we find a distribution in the CML-Io phase plane that is very similar to what is observed from Earth in the same frequency range. For longitudes less than 200° we see that most of the events occur at Io phases near 90° corresponding to the Io-related "early" or "B" source, and there are relatively few events at other Io phases. For longitudes above 200°, we find a large number of events spread over all values of Io phase. There is evidence for a concentration of activity centered near 240° Io phase corresponding to the Io-related "main" (A) and "late" (C) sources. Io-related decametric activity generally extends to higher frequencies than do Io-independent events, and thus the events which were observed to reach maximum frequencies above 30 MHz have a particular tendency to clump in the regions of the diagram that have long been associated with Io-related

emission. The Io-related "fourth" or "D" source seen in ground-based surveys at longitudes between 0° and 100° for Io phase near 105° is not evident in Figure 4 because that component is never observed to extend to frequencies as high as 20 MHz. When we compare the Voyager pre-encounter data collected from above the morning sector of Jupiter and displayed in Figure 3 and 4 with similar compilations of ground-based observations there is no evidence for any differences that can be attributed to the small local time differences in the data sets.

The post-encounter data (right-hand panels in Figure 4) reveal an important difference when compared to the pre-encounter observations. We see a much larger number of Io-independent events at longitudes less than 200° and a substantial drop in the incidence of Io-independent activity at longitudes above 200°. Thus the marked reversal in the relative levels of decametric activity at early and late longitudes that occurred when the Voyagers passed into the night hemisphere of Jupiter (Figure 3) is attributable to changes in the Io-independent component of the emissions. When we use location in the CML-Io phase plane and dynamic spectral characteristics (see Boischot et al. [this issue]) as joint criteria to identify Io-related events, we find essentially equal numbers of Io-related events before and after encounter. Indeed, there is no clear evidence in these data for a change either in the locations in Io-phase and longitude or in the occurrence probability of Io-related decametric events after Voyager encounter.

The counts of Io-related decametric events reveal another interesting aspect of this component of the emissions—namely, a very high absolute occurrence probability. Using the definitions given by Carr and Desch [1976] for the four Io-related "source" locations in the CML-Io phase plane, we examined the Voyager data within $\pm$ 10 days of each encounter for evidence of Io-related activity at frequencies above about 15 MHz on every occasion when the CML and Io phase were within $\pm$ 45° and $\pm$ 10°, respectively, of their preferred values. Distinct Io-related emissions were observed to occur on 95% of all such cases (38 events out of a possible 40 opportunities). Thus we suspect that when the geometry is favorable the occurrence probablity for Io-related decametric emission is essentially 100% just as was predicted by Dulk [1965]. Occurrence probabilities approaching this maximum value are only

observed from Earth in the "centers" of the Io-related sources and then only in years of maximum jovicentric latitude of Earth. More typical ground-based values of occurrence probability near the Io-related zones of the longitude-Io phase diagram are ≈ 60%. This is most likely a sensitivity effect; the greater sensitivity of the Voyager instruments near Jupiter permit the detection of emission that would not always be readily observed with the typical radio telescopes used for monitoring Jupiter from Earth. The apparent sporadic occurrence of decametric emissions even when the geometry is favorable for observing Io-related activity from Earth must be due to intensity variations rather than to occasional cessation of the emission.

III. FLUX DENSITY DISTRIBUTIONS

Another method for portraying the statistical dependence of Jovian activity on CML has been utilized which is complementary to the superposed dynamic spectra and the occurrence probability histograms. It consists of histograms of average flux density at a given frequency plotted as a function of CML or Io's orbital phase.

In this method the stronger events contribute more to the synoptic histogram than do the weaker ones. In some important respects, this is advantageous for investigating beaming effects, since events occurring when the Jovian emission beam is more nearly centered on the receiving antenna tend to be more intense than those received farther out in the beam. Ellis and McCulloch [1963] first demonstrated that the use of average flux density instead of occurrence probability tends to intensify characteristic histogram peaks. Bigg [1964] made use of this effect to accentuate the peaks indicative of Io's control.

The preparatory data processing and plotting of average flux density histograms was computer-controlled, except for an editing stage in which bad sections of data (and type III solar bursts) were identified by an operator and deleted. Since even a few wild points might badly contaminate the flux density averages, it was essential that they be removed. The operator also selected for each of the two senses of circular polarization on each frequency channel a short segment of relatively undisturbed baseline from each 24-hr

data run. The average of the values in such a baseline segment was then subtracted from each of the data points in the 24-hr run in order to eliminate insofar as possible the constant background noise component. The background noise consisted almost entirely of interference generated within the spacecraft. Any non-CML-modulated Jovian continuum, had there been any, would have been indistinguishable from the background and would have been eliminated by the subtraction. At times, abrupt changes in baseline level occurred due to the switching on or off of some instrument in the spacecraft. In such cases it was necessary for the data editor either to delete the affected section or to make a new baseline calibration. On some channels, particularly in the high-frequency band, the baselines were so unstable that the channels were unusable. Since the various flux density measurements used in a given histogram were made when the spacecraft was at different distances from Jupiter, all such measurements were inverse-square-adjusted to a standard distance.

Two of the average flux density histograms, for 10.1 and 18.4 MHz, are shown in the top panels of Figure 5. The LH and RH polarization components have been combined. It is significant that the peak centered on 40° CML in the 10.1 MHz histogram was composed of almost pure LH circularly polarized radiation, while that centered at about 200° was almost pure RH. The rotation senses of the electric vector of the wave in these two cases correspond to those of the extraordinary propagation mode near the south and north magnetic dipole axes (which are tipped toward the 20° and 200° longitude meridians), respectively. Such an effect at 10 MHz had been demonstrated previously, but less clearly, by Kennedy [1969] from ground-based measurements. The characteristic peaks known as sources B and A are prominent in the 18.4 MHz histogram; the shoulder following the A peak is all that can be seen of source C.

For comparison, occurrence probability histograms obtained from ground-based measurements at nearly the same two frequencies are presented at the bottom of Figure 5. The two 18 MHz histograms are very similar, except for the difference of about 10° in the CML of the source A peak. There is a much greater difference in the two 10 MHz histograms. Plots of occurrence probability and average flux density do not necessarily coincide completely, but that distinction alone does not seem adequate to explain the differences

in the 10 MHz plots. Although we will show later that the structure of histograms obtained in the vicinity of 10 MHz is so strongly dependent on spacecraft latitude that a 3.5° difference alters their shapes radically, the latitude difference in Figure 5 was only about a degree. The possibility exists that the 10 MHz histogram structure varies with time as well as latitude.

In Figure 6, histograms of average flux density vs. CML for V1 and V2 pre-encounter data are compared at several frequencies. Both polarization components are displayed. Most of the differences in corresponding pairs of histograms are believed to have been due to the 3.5° difference in the Jovicentric latitudes of the two spacecraft. For example, the difference in the width of the valley centered on 220° CML in panel c from that in d, and also the difference seen in panels e and f, is probably due to the latitude effect. V2, which was at the higher latitude, shows the wider valley in both cases. As we noted earlier, this is consistent with the conical-sheet beaming model proposed by Alexander et al. [1979] for the hectometric emission.

The morphological difference which is apparent in panels g and h is even more striking. Panel h shows the same type of bimodal lobe and polarization structure which is apparent in the 10.1 MHz V1 histogram in Figure 5. On the other hand, no trace of the large LH peak at 30° is found in the histogram of panel g; instead, a large RH peak has appeared at 310° and the 210° RH peak has diminished in size. It is true that there is a slight difference in the frequencies of g and h. However, comparisons with histograms at neighboring frequencies have shown conclusively that the structural differences in g and h cannot be due to this frequency difference. A somewhat similar difference is apparent in i and j. Panels k and l, at 18.432 kHz, show the customary RH polarized decametric sources B and A, but with slight differences which could be due to the latitude difference. Panel b shows the typical tapered peak centered near 200° which is characteristic of the broadband kilometric radiation. The additional peaks in a could be due to strong narrow-band kilometric events, which are not so restricted in CML.

Both the hour-angle effect and the latitude effect are apparent in Figure 7. In the pre-encounter histograms of columns a, b, and c, the 220° valley is

wider for the higher latitude spacecraft (V2, at 6.7° latitude) than for the one at lower latitude (V1 at 3.2°), just as it was for the 788 and 1307 kHz histograms in Figure 6. For the post-encounter histograms in Figure 7, on the other hand, the two spacecraft were at essentially the same latitude (5.1° and 4.7° for V1 and V2, respectively), which by coincidence was very nearly the mean of the two pre-encounter latitudes. It is clear from column a of Figure 7 that the 961 kHz flux density distributions recorded from the two spacecraft during the specified post-encounter periods were almost identical, both in shape and magnitude, despite the four-month time difference. In this case, no latitude effect would be expected. Furthermore, if there had been no difference between the emission from the sunlit side and the dark side of Jupiter, both post-encounter histograms would have been intermediate in shape between those of the two pre-encounter ones. But this was not the case. The marked differences of the post-encounter histograms from the pre-encounter mean must be attributed to the hour-angle effect. A similar situation exists for the histograms in columns b, c, and d of Figure 7.

The variation of average flux density with respect to both CML and Io's orbital phase are displayed for a wide range of frequencies in Figure 8. The flux density measurements were made from V2 over a 31-day period after encounter, and as usual, were adjusted to a standard distance. The first and third columns clearly show the frequency evolution of CML histogram morphology from 22.4 MHz down to 443 kHz. Histograms for frequency channels between 7066-2765 kHz were not included because of excessive baseline instability.

From 22,426 kHz down to 12,595 kHz, the source B peak drifts to higher values of CML. The source A peak also does so, but at a slower rate, and the two peaks begin to merge as they both broaden. At 8602 kHz, B and A have consolidated into a single large peak centered at about 320°. This peak is still dominant at 2765 kHz. At 1843 kHz a second peak centered on about 90° has appeared. The two peaks then form the distinctive hectometric valley centered on 220°, which is most prominent between 1843 kHz and 788 kHz. Thus we see the same trends in flux density as a function of frequency and CML as were observed in the occurrence probability plots in Figure 2. As previously noted, the width of the hectometric valley at a fixed frequency increases as the spacecraft latitude increases from 3.2° to 6.7°. We now note that at a

fixed latitude, the valley widens with decreasing frequency. The valley is apparently a permanent feature, and its dimensions at the various frequencies can be measured precisely from our histograms. It should be possible to use these plots to construct a model of emission beam shape as a function of frequency, and when suitable ray tracing facilities are utilized, to expand the model to include plasma distributions within the part of the Jovian magnetosphere through which the radiation propagates.

The second and fourth columns of Figure 8 demonstrate the effect of Io. From 22,426 kHz down to 7066 kHz the customary peaks centered on 90^{o} and 240^{o} from superior geocentric conjunction are apparent. In the same type of histograms plotted from a sufficient quantity of terrestrially-recorded data, the two peaks would have been much sharper at 22 and 18 MHz, but below about 15 MHz would probably have been much less apparent than the corresponding ones in Figure 8. And, of course, no reliable results at all have been obtained from ground-based observatories below about 9 MHz because of terrestrial ionospheric effects.

Both peaks are still discernable at 2765 and 1843 kHz (Figure 8, fourth column), although they are less clearly defined than at the higher frequencies. The peaks appear to start disintegrating at about 1307 kHz, but they seem to return at 616 and 443 kHz. These are lower frequencies than any at which Io control has previously been detected. Desch and Carr [1978] had observed the two Io peaks at 2200 kHz with RAE-1 data, and M. D. Desch [private communication] found from IMP-6 data that evidence for Io control could not be tracked below 1300 kHz. Kaiser et al. [1979] found no evidence of Io control in their study of Jupiter activity below 1.3 MHz early in the cruise phase of the two Voyagers. We consider the evidence for an Io effect at the two lowest frequencies to be ambiguous, and so a confirmation or resolution of this interesting question must await the completion of further Voyager data analyses.

IV. POLARIZATION PROPERTIES

Using the same one-month pre- and post-encounter data sets that formed the basis for the occurrence probability summaries in Figure 2, we have calculated

the average indicated axial ratio measured by V2 as a function of frequency and CML before and after Jupiter encounter. The results are shown in Figure 9. The sign of the axial ratio is denoted by a grey-shading scheme which varies from white, representing left-hand (LH) polarization, through black, representing right-hand (RH) polarization. An axial ratio of zero (corresponding to unpolarized or linear polarized waves or to no signal) is indicated by the shade of grey most prevalent in the figure. A non-zero value of the axial ratic is displayed for a given frequency in Figure 9 only in those 1° longitude bins for which there were at least 10 events at intensity levels more than 1 dB above background during the one-month averaging interval.

In the DAM frequency range above 15 MHz we see that before encounter the polarization is predominantly RH. After encounter, an unfavorable antenna geometry makes the determination of polarization at frequencies above 15 MHz less sensitive, and thus there is little polarization information in the post-encounter average axial ratio plot for the high frequency range. However, from a detailed inspection of the individual spectra of the events that were used to compile Figures 3 and 4 we find that more than 90% of all DAM events that extend to frequencies $\geq$ 20 MHz are RH polarized. This is consistent with ground-based polarization measurements that show LH polarized emissions only at frequencies below $\sim$20 MHz. Narrow frequency bands near 5, 15 and 25 MHz where the indicated polarization is weak or even reverses are due to antenna resonances and/or antenna pattern nulls that limit the polarization discrimination of the PRA system at those frequencies. Between about 5 and 15 MHz where we find activity extending across almost all longitudes, a very well organized polarization pattern occurs. LH polarization is observed from 0° to 135° CML and RH polarization is observed from 135° to 300°. Both polarizations appear between 300° and 360°, but comparison with Figure 2 shows that the region of higher probability is RH polarized. This pattern is basically the same both before and after encounter, although as we noted earlier the relative amount of activity near 10 MHz at early longitudes decreases after encounter.

The polarization patterns observed at HOM wavelengths in the low frequency band of the PRA receiver are more complex. In some parts of the CML-frequency plane the predominant polarization sense may have reversed after

encounter. For example, before encounter, the polarization at frequencies between 1.3 and 0.5 MHz is RH at longitudes from 350° to 70°, but after encounter this region of Figure 9 shows LH or mixed polarization. There are broad, drifting patterns of alternating LH and RH polarization at high longitudes in Figure 9 that correspond roughly to the drifting lane features in the occurrence probability maps in Figure 2, but the polarization patterns are not the same before and after encounter. Whether the changes correspond to a polarization reversal or to a shift in longitude or frequency of a given feature is not clear. Some of the changes in the average HOM polarization patterns are probably due to the local time variations of the relative occurrence probability and intensity of the various DAM arc families that extend into this low frequency range. Emissions which occur with one preferred polarization sense may dominate before encounter but may become secondary to a different class of emissions having the opposite polarization sense after encounter.

The bKOM radiation is easily distinguished from the HOM emission at frequencies below 500 kHz where it partially fills the gap in the HOM radiation between longitudes of 130° and 270°. The reversal in the polarization of bKOM reported by Desch and Kaiser [1980] is especially clear. The bKOM radiation is consistently LH polarized before encounter and RH after encounter.

V. FLUX DENSITY SPECTRUM

The average power flux density over all values of CML at a given frequency can easily be found from the histogram for that frequency. This was done for a wide range of frequencies for V1 and V2 before encounter. The resulting average flux density values are plotted as a function of frequency in Figure 10. When suitable data were available from both spacecraft at the same (or nearly the same) frequency, the individual values and their averages are plotted. Where only the point for one spacecraft has been plotted, the omission of the other was usually due to evidence of baseline instability. Circles denote V1 data and triangles denote V2. The outstanding features of this spectrum are a peak between 3 and 14 MHz, a shoulder extending from 3 MHz down to 800 kHz, and a deep minimum at 200 kHz. The well-known steep decline

above about 12 MHz is very apparent. Although it does not appear in this figure, there is also a steep decline below 20 kHz (Scarf et al., 1979), due to the fact that the plasma frequency along the early portion of the propagation path may be as high as 3 kHz or more. At frequencies above about 2 MHz, the shape of the average flux density curve in Figure 10 is about the same as the peak flux density curve of Carr and Desch [1976], the latter being about an order of magnitude higher. It is interesting to note that the secondary maximum exhibited by the so-called "mid-frequency" events of Brown [1974] occurred at about 1 MHz, within the shoulder of the curve in Figure 10.

By integrating a curve fitted to the points in Figure 10, we can obtain for the first time a realistic estimate of the low frequency radio power per unit area from Jupiter based on a nearly complete measured spectrum, and from that the total emitted power derived on the assumption that radiation from the planet is isotropic. Our results indicate that the average power emitted at all frequencies below the 40 MHz cutoff is 8.4×10^{-14} W/m^2 at 4 AU, corresponding to 3.8×10^{11} W total power (assuming isotropy). The isotropic equivalent total power in the hectometric band alone, between 300 kHz and 3 MHz, is 3×10^{10} W, and in the kilometric band alone, below 300 kHz, is 3×10^{8} W. Desch and Kaiser [1980] obtained 8×10^{8} W for the isotropic equivalent total power for the broadband kilometric component. After accounting for the fact that Desch and Kaiser computed the "most probable" flux density observed when the bKOM was "on" but that we compute the averge flux density over all times and longitudes, the two total power estimates are completely consistent.

We have estimated the isotropic equivalent synchrotron emission power from Jupiter at frequencies between about 100 and 12000 MHz to be approximately 2×10^{9} W, based on data presented by Berge and Gulkis [1976]. This is less than 1% of the low frequency radio power. The ultimate source of the synchrotron power is probably the solar wind, the power transfer being via inward diffusion of accelerated charged particles into the radiation belts. It is possible that the low frequency radio emission obtains its power in the same way. The solar wind power flux carried toward the cross sectional area of Jupiter's magnetosphere is about 6×10^{14} W [Nishida et al., 1967]. Although only a small fraction can reach the inner magnetosphere, there might be enough

to supply the necessary 4×10^{11} W without the need of assuming an unrealistically high conversion efficiency.

An alternative possibility for the energy source is Jupiter's rotational kinetic energy. There are several ways in which energy from the corotating magnetosphere might be converted into particle or Alfven wave energy by its motion past Io, or by the acceleration of photo-ionized volcanic ejecta from Io or of photo-ionization ascending from the Jovian ionosphere. Staelin [this issue] has proposed one such mechanism as the source of the low frequency radio emission. Newly photo-ionized volcanic ejecta is accelerated as it becomes locked about magnetic flux tubes. Staelin estimates 3×10^{12} W as the power acquired by these particles. They are assumed subsequently to emit the radio waves. The efficiency of conversion of particle to electromagnetic energy would have to be $(4 \times 10^{11})/(3 \times 10^{12})$, or about 13%. This seems unrealistically high, however. A. J. Dessler [private communication] has estimated that an upper limit to the power available from the release of centrifugal potential energy to drive magnetospheric convection is 5×10^{13} W. Sandel et al. [1979] suggest that the electrons originating in the torus which create the Jovian aurora as they precipitate into the atmosphere have a power of about 1.7×10^{14} w. This is 400 times greater than the radio power; perhaps these same electrons, or related ones, emit the radio waves. Although it is not completely clear whether this power is derived from the solar wind or from Jupiter's rotation, we believe that the Io plasma torus and the rapid rotation of Jupiter's inner magnetosphere have to play key roles in the radio emission as well as in many other magnetospheric phenomena.

VI. SUMMARY AND CONCLUSIONS

The principal findings of our synoptic survey of the average statistical properties of Jupiter's radio emissions can be summarized as follows:

1. Decameter-wavelength (DAM) occurrence probability profiles as a function of CML and Io phase obtained by Voyager from above the dayside hemisphere of Jupiter are essentially identical to those obtained from Earth. We find no evidence for statistical differences that can be attributed to the difference of up to $\sim$ 2.5 hr in observer's hour

angle between Voyager before closest approach and typical ground-based observations.

2. Io-related DAM is always observed (100% occurrence probability) when the combination of observer's CML and Io phase coincides with one of the four zones into which the Io-related DAM has traditionally been sub-divided. This persistent geometrical pattern is the same after encounter as before and does not appear to depend on local time. The sporadic occurrence of the Io-related DAM noted in Earth-based catalogs must be a consequence of variations in event intensity at different times.

3. In constrast to the Io-related DAM, Io-independent emissions at frequencies above 20 MHz exhibit marked local time effects. The zone of high occurrence probability at CML $\sim 260^{\circ}$ observed from above the day hemisphere of Jupiter becomes suppressed after encounter and is replaced by an occurrence probability maximum at CML $\sim 160^{\circ}$ for observations collected from above the nightside of the planet. The emission at high longitudes does not vanish entirely after encounter, but it tends to occur at lower flux levels. Thus the variations in relative occurrence probability with observer's hour angle may be primarily a consequence of a dependence of emission intensity on local time.

4. The preferred sense of polarization (RH) for both Io-related and Io-independent DAM at frequencies above 20 MHz remains unchanged after encounter.

5. DAM in the frequency band from a few MHz to $\sim$ 15 MHz, where dynamic spectral lesser arcs prevail, exhibits a distinct, essentially bi-modal pattern in sense of polarization versus CML. The average axial ratio and polarized flux density profiles both show the emission near 10 MHz to be LH polarized between 0° and 135° CML and RH polarized between 135° and 300°.

6. Both the LH polarized flux density and the occurrence probability of

emission at frequencies near 10 MHz decrease after encounter for longitudes below about 140^{o}. Thus there is evidence of local time effects for lesser-arc DAM emission as well as for higher frequency great-arc DAM. (See also Leblanc and Daigne [this issue].)

7. Flux density profiles as a function of CML at frequencies near 7 to 10 MHz appear to vary strongly with observer's latitude and/or with time.

8. At frequencies near 1 MHz and below corresponding to hectometric (HOM) wavelengths, there are differences in the two pairs of Voyager data sets that appear to be due to both observer's local time and a strong latitude dependence.

9. Displays of average sense of polarization as a function of frequency and CML at HOM wavelengths exhibit complex drifting patterns that are reminiscent of similar features in frequency-CML plots of occurrence probability. Changes in both types of displays after encounter provide further evidence of a local time effect in the generation and/or propagation of Jupiter's emissions at HOM wavelengths.

10. There is evidence for some influence by Io on the emission flux density down to at least 1.8 MHz. If this emission is generated near the electron gyrofrequency on Io-threaded field lines, then the Io-related sources must occur over Jovicentric radial distances ranging from just above the cloud tops to $\sim 3\ R_J$.

11. The average power flux density spectrum of Jupiter's radio emission observed by Voyager has a broad peak between between 5 and 10 MHz. The sharp high frequency fall-off between 30 and 40 MHz observed from Earth is confirmed. At low frequencies, this emission component extends to below 100 kHz. The average flux density spectrum of the KOM component rises with decreasing frequency with a power-law index, $S = \text{const.} \times f^{-\alpha}$, of $\alpha \sim 2$. The average isotropic equivalent emission power integrated over all frequencies below 40 MHz is 4×10^{11} W; within the HOM band alone it is 3×10^{10} W; and within the KOM band alone it is 3×10^{8} W. The low frequency radio power is about 200

times that of the synchrotron emission but only 1/400 that of the auroral UV emission.

The CML profiles for DAM emission at frequencies $\geq$ 20 MHz are all consistent with the simple "lighthouse" model of a radio source which remains essentially fixed in a limited latitude and longitude region and which rotates with the planet. The observed frequency range and the predominance of RH polarization sense are also consistent with earlier models in which the emission escapes from the northern hemisphere in the extraordinary mode at frequencies near the source electron gyrofrequency. The Voyager data suggest that the Io-controlled events must depend purely on the location of Io with respect to the source region (to meet conditions necessary for stimulation of the emission) and on the orientation of the source with respect to the observer (to meet conditions necessary for reception of the emission). In view of the similarities in dynamic spectral characteristics and in location in CML for both the Io-controlled and Io-independent DAM, the latter emissions must come from nearly the same locations as the Io-controlled DAM. The slightly lower high-frequency limit for the Io-independent events may be a consequence of a slightly different range of L-shells for the source field lines or, perhaps, a consequence of the penetration of the energy source for Io-controlled DAM to slightly lower ionospheric altitudes (and higher gyrofrequencies) than for Io-independent emission.

The reversal in the longitude of the primary and secondary activity peaks for the Io-independent emission is very probably a local time effect. That is, the occurrence probability distribution for Io-independent great-arc events depends on the location of the source and/or the observer with respect to the Jupiter-sun line.

To illustrate how this local time dependence for the Io-independent emissions may occur, let us consider the conical beam model often discussed to explain the DAM emissions [Pearce, this issue; Staelin, this issue; Goldstein and Thieman, this issue]. In such a model, radio emission at a given frequency is beamed at an oblique angle with respect to the magnetic field at the source so as to form a radiation pattern in the shape of a hollow conical sheet. In the context of the data shown in Figure 3 the occurrence

probability minimum at approximately 200° longitude defines the location of the cone axis, and the peaks centered near 160° and 260° correspond to the rotation of the leading and trailing edge of the emission cone across the observer's line of sight.

The circumstances of this model for the Voyager observations are illustrated in their simplest form in Figure 11. In the upper diagrams we show the orientation of the conical beam with respect to Voyager before encounter. When the early longitude (160°) activity peak is observed the emission cone (and, presumably the radio source) is situated in the morning hemisphere near the dawn meridian. When the later longitude peak (260°) is observed the source cone is located in the early afternoon local time sector. The post-encounter geometry is illustrated in the lower pair of diagrams. In this case, Voyager observes activity at early CML when the emission cone is located over the midnight sector, and the late longitude emissions are detected when the source cone is in the morning hemisphere. Notice that both before encounter and after encounter when the secondary activity peak is observed (160° before encounter, 260° after encounter) we find the same location in local time for the source cone—near the dawn sector.

Thus, for the model sketched in Figure 11 the probability of observing Io-independent great arcs above 20 MHz is apparently suppressed when the emission is beamed from above the dawn local time region. There may be other equally plausible models, but in any case, the Voyager data indicate that there exist significant Jupiter-sun line orientation effects which operate to regulate the emission generation mechanism and/or the radiation pattern and propagation. In the case of the emission mechanism, such an effect could be due to local time variations in the energy source, in the path between the energy source and the radio source, or in the coupling mechanism by which energy is converted into decametric waves. We note that Voyager ultraviolet observations of the Io plasma torus suggest that there may be a dawn-dusk asymmetry in the torus electron temperature profile [Sandel et al., this issue], and such an asymmetry could affect the details of the role of the plasma torus in the DAM emission process as a function of local time. The DAM radiation pattern and propagation paths could be expected to depend on local time as a consequence of variations in absorption, refraction, or occultation

or due to changes in the topology of the magnetic field which could tilt the emission beam out of view for certain observer orientations. One likely site for the explanation of the local time effects observed by Voyager is the Jovian ionosphere, because we can expect that ionospheric density, scale height, and conductivity could all show variations with local time. These changes could, in turn, manifest themselves in changes in the properties of the radio emissions observed from above different local time sectors. For example, in the emission mechanism developed by Goldstein and Eviatar [1979], longitudinal gradients in the magnetic field or electron density distribution can determine how long a wave will propagate in the region where significant wave growth occurs before being refracted out of the amplification region. In such a model we might therefore expect to observe significant differences in the amplification, and hence in the intensity levels, for opposite sides of an emission cone. Alternatively, in the context of the multiple Alfven wave reflection model of Gurnett and Goertz [this issue], a drop in ionospheric conductivity near the dawn sector could be expected to limit the reflectivity for Alfven waves in the dawn ionosphere and thereby reduce the number of discrete source locations available for the generation of DAM in that local time zone.

Acknowledgments

We are pleased to acknowledge the contributions by J. W. Warwick, Principal Investigator, and our other colleagues on the Planetary Radio Astronomy Team. We are especially grateful to M. D. Desch and M. L. Kaiser for numerous discussions and to P. G. Harper and E. M. Rodriguez Kuiper for assistance with the data analysis. The work of JRT has been supported, in part, by NASA contract NAS5-25932.

References

Alexander, J. K., M. D. Desch, M. L. Kaiser, and J. R. Thieman, Latitudinal beaming of Jupiter's low frequency radio emission, J. Geophys. Res., 84, 5167, 1979.

Berge, G. L. and S. Gulkis, Earth-based radio observations of Jupiter: Millimeter to meter wavelengths, Jupiter, edited by T. Gehrels, p. 621, University of Arizona Press, Tucson, 1976.

Bigg, E. K., Influence of the satellite Io on Jupiter's decametric emission, Nature, 203, 1008, 1964.

Boischot, A., A. Lecacheux, M. L. Kaiser, M. D. Desch, J. K. Alexander, and J. W. Warwick, Radio Jupiter after Voyager: A radio astronomy overview, J. Geophys. Res., this issue, 1981.

Brown, L. W., Spectral behavior of Jupiter near 1 MHz, Astrophys. J. (Lett.), 194, L159, 1974.

Carr, T. D., and M. D. Desch, Recent decametric and hectometric observations of Jupiter, Jupiter, edited by T. Gehrels, p. 693, University of Arizona Press, Tucson, 1976.

Desch, M. D., and T. D. Carr, Modulation of the Jovian emission below 8 MHz, Astron. J., 83, 828, 1978.

Desch, M. D., and M. L. Kaiser, The occurrence rate, polarization character, and intensity of broadband Jovian kilometric radiation, J. Geophys. Res., in press, 1980.

Dulk, G. A., Io-related radio emission from Jupiter, Ph.D. dissertation, University of Colorado, Bolder, CO, 1965.

Dulk, G. A., and T. A. Clark, Almost-continuous radio emission from Jupiter at 8.9 and 10 MHz, Astrophys. J., 145, 945, 1966.

Ellis, G. R. A., and P. M. McCulloch, The decametric radio emissions of Jupiter, Australian J. Phys., 16, 380, 1963.

Goldstein, M. L., and A. Eviatar, An emission mechanism for the Io-independent Jovian decametric radiation, Astrophys. J., 230, 261, 1979.

Goldstein, M. L., and J. R. Thieman, On the formation of arcs in the dynamic spectra of Jovian decameter bursts, J. Geophys. Res., this issue, 1981.

Gurnett, D. A., The Earth as a radio source: Terrestrial kilometric radiation, J. Geophys. Res., 79, 4227, 1974.

Gurnett, D. A., and C. K. Goertz, Multiple Alfven wave reflections excited by Io: Origin of the Jovian decametric arcs, J. Geophys. Res., this issue, 1981.

Kennedy, D. J., Polarization of the decameter radiation from Jupiter, Ph.D. dissertation, University of Florida, Gainesville, FL, 1969.

Kaiser, M. L., M. D. Desch, A. C. Riddle, A. Lecacheux, J. B. Pearce, J.K. Alexander, J. W. Warwick, and J. R. Thieman, Voyager spacecraft radio observations of Jupiter: Initial cruise results, Geophys. Res. Lett., 6, 507, 1979.

Leblanc, Y., and G. Daigne, On the arc structure of the DAM Jupiter emission, J. Geophys. Res., this issue, 1981.

Lecacheux, A., B. Pedersen, A. C. Riddle, J. B.. Pearce, A. Boischot, and J. W. Warwick, Some spectral characteristics of the hectometric Jovian emission, J. Geophys. Res., in press, 1980.

Nishida, A.. K. Maezawa, and T. Terasawa, Energetics of terrestrial and Jovian magnetospheres, Space Sci. Rev., 23, 345, 1979.

Pearce, J. B., A heuristic model for Jovian decametric arcs, J. Geophys. Res., this issue, 1981.

Sandel, B. R., D. E. Shemansky, A. L. Broadfoot, J. L. Bertaux, J. E. Blamont, M. J. S. Belton, J. M. Ajello, J. B. Holberg, s. K. atreya, T. M. Donahue, H. W. Moos, D. F. Strobel, J. C. McConnell, A. Dalgarno, R. Goody, M. B. McElroy, and P. Z. Takacs, Extreme ultraviolet observations from Voyager-2 encounter with Jupiter, Science, 206, 966, 1979.

Scarf, F. L., D. A. Gurnett, and W. S. Kurth, Jupiter plasma wave observations: An initial Voyager 1 overview, Science, 204, 979, 1979.

Staelin, D. H., Models for the origin of Jovian decametric emission, J. Geophys. Res., this issue, 1981.

Thieman, J. R., A catalog of Jovian decameter radio observations from 1957-1978, NASA Goddard Space Flight Center TM-80308, 1979.

Figure Captions

Fig. 1. Comparisons of the coverage in local time (upper plot) and in jovigraphic latitude (lower plot) afforded by Voyager-1 and 2 and by Earth-based observations. Earth and the sun are off to the left-hand side of each diagram.

Fig. 2. Color-coded diagrams of average radio emission occurrence probability as a function of frequency and central meridian longitude for observations from Voyager-1 (above) and Voyager-2 (below) for one-month intervals before (left) and after (right) each encounter.

Fig. 3. Comparison of longitude histograms of the probability of occurrence of decametric activity observed from Earth at 22.2 MHz during the 1976 apparition (top) and of decametric activity observed by Voyager-1 (middle) and Voyager-2 (bottom) at frequencies above 20 MHz. The longitude of the main histogram peak in the Voyager data before encounter (solid lines) is the same as in the ground-based histograms, but after encounter (dashed lines) the longitude profile clearly changes.

Fig. 4. Plots of the occurrence of decametric emission at frequencies above 20 MHz observed by Voyager-1 (above) and Voyager-2 (below) for one-month intervals before (left) and after (right) encounter as a function of central meridian longitude and Io phase. The heavy lines denote those events that extended to 30 MHz or higher.

Fig. 5. Comparisons of pre-encounter Voyager-1 measurements of average flux density (adjusted to a standard distance) vs. Jovian CML with ground-based measurements of occurrence probability vs. CML at nearly the same frequencies. The two peaks in the upper right histogram represent almost completely circularly polarized radiation of opposite senses, as indicated.

Fig. 6. Illustrations of the Jovian latitude effect. Ordinates are equivalent flux densities at 0.1 AU in units of 10^{-19} W m^{-2} Hz^{-1}. The LH and RH circularly polarized components are indicated by dashed and solid lines, respectively. V1 and V2 measurement periods were February 21

through March 3, 1979, and June 24 through July 7, 1979, respectively. The mean spacecraft latitude for the V1 measurements was 3.2° and for V2 was 6.7°. The lowest point on the LH and RH histogram pair was taken to be the zero of the flux density scale.

Fig. 7. Illustrations of the Jovian hour-angle effect. Ordinates are proportional to equivalent 0.1 AU average flux densities, but scales are different for the different histograms. LH and RH components have been combined. V1 and V2 post-encounter measurement periods were March 7 through March 24, 1979, and July 13 through July 26, 1979; pre-encounter measurement periods were the same as in Fig. 6. Mean spacecraft latitudes were: V1 pre-encounter, 3.2°, V2 pre-encounter, 6.7°; V1 post-encounter, 5.1°, and V2 post-encounter, 4.7°. The lowest point on the histogram was taken to be the zero of the flux density scale.

Fig. 8. Voyager 2 post-encounter measurements of average flux density (adjusted to a standard distance) vs. Jovian CML and vs. Io orbital phase for the period July 13 through August 12, 1979, for each of a wide range of frequencies. Flux density scales are linear, but are not the same for the different frequencies.

Fig. 9. Grey-shaded diagram of the average axial ratio measured by Voyager-2 before (above) and after (below) encounter as a function of central meridian longitude. Right-hand polarization is indicated by black, and left-hand polarization is indicated by white. Regions of the diagram which appear as a grey background correspond to areas of very low occurrence probability or unpolarized emission.

Fig. 10. Average flux density spectrum (over all values of CML) derived from V1 and V2 measurements before encounter. Open circles indicate data from V1 only; open triangles indicate data from V2 only; and black-filled circles denote the average from both spacecraft. Measurement periods for V1 and V2 were February 18 through March 3, 1979 and June 24 through July 7, 1979, respectively. LH and RH flux densities have been combined. Plotted values are relative to the lowest point on the corresponding CML histogram.

Fig. 11. A simplified schematic view of the possible locations in local time for a source from which DAM emission is beamed into a hollow conical sheet. Opposite sides of the cone could contribute to the two histogram peaks of Fig. 3.

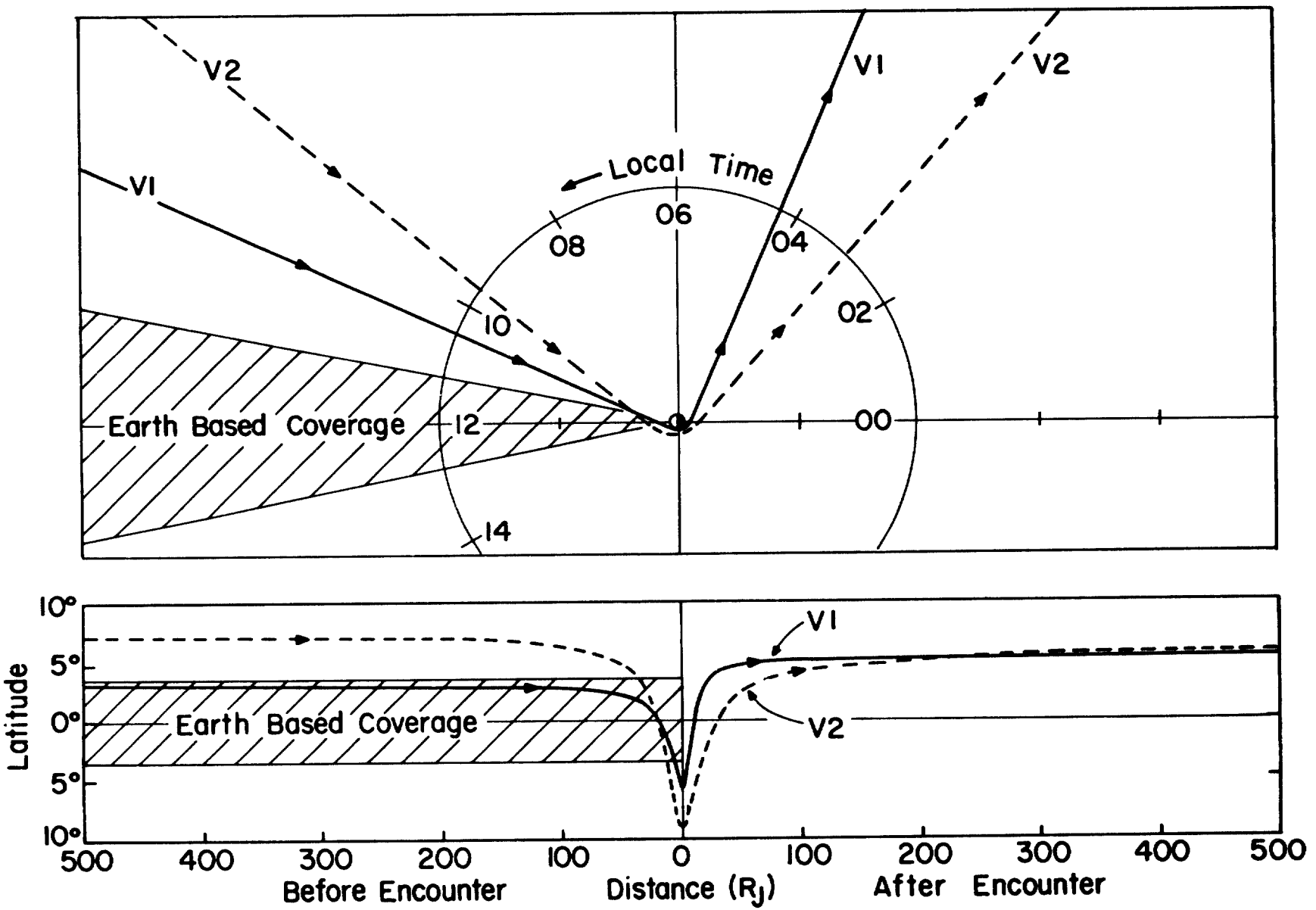
V2
V1
V2
V1
Local Time
06
08
04
10
02
Earth Based Coverage
12
00
14
10°
5°
0°
5°
10°
Latitude
V1
Earth Based Coverage
V2
500
400
300
200
100
0
100
200
300
400
500
Before Encounter
Distance (Rj)
After Encounter

Fig. 1

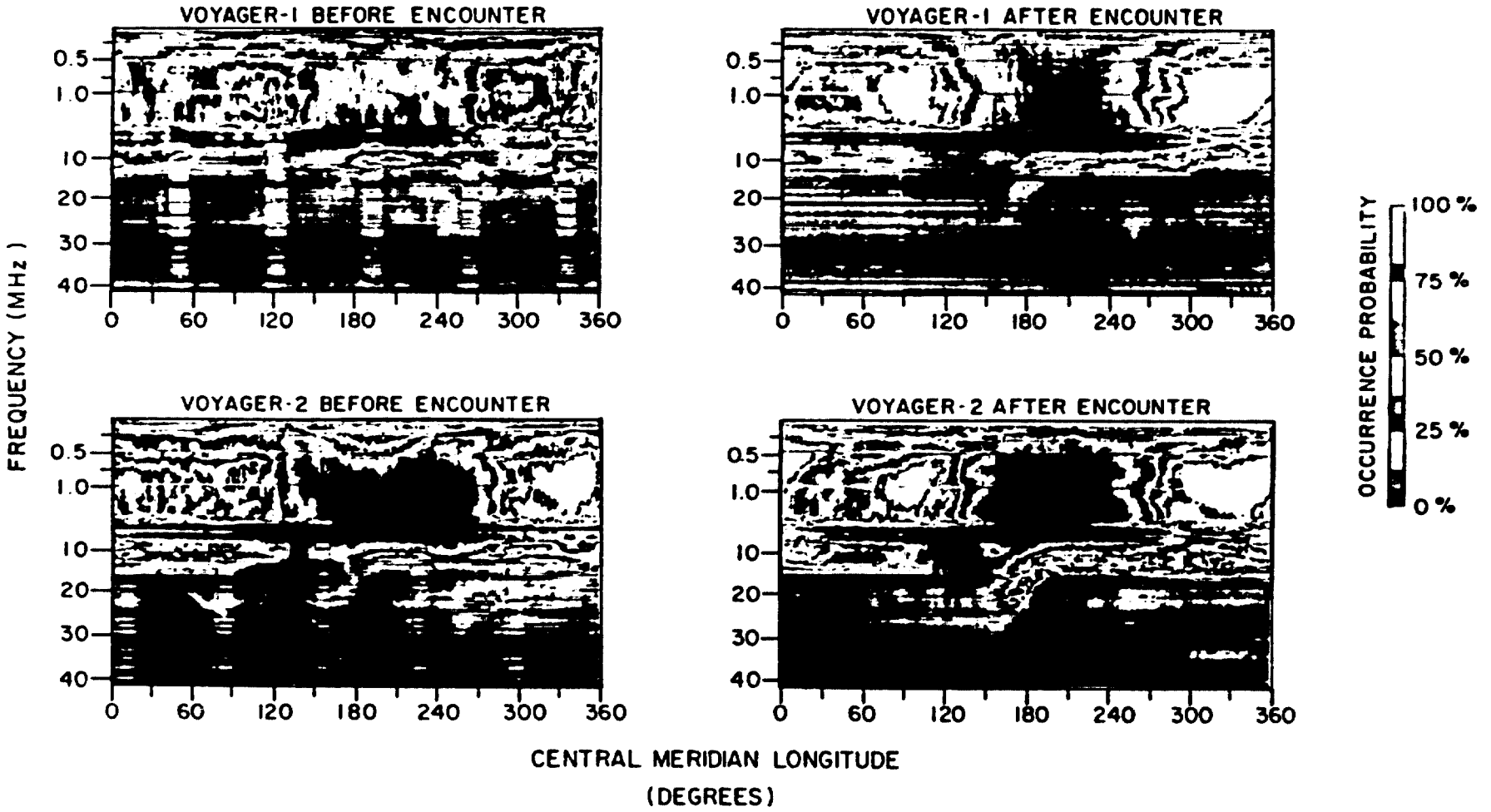
VOYAGER-1 BEFORE ENCOUNTER
VOYAGER-1 AFTER ENCOUNTER
VOYAGER-2 BEFORE ENCOUNTER
VOYAGER-2 AFTER ENCOUNTER
FREQUENCY (MHz)
0.5
1.0
10
20
30
40
0
60
120
180
240
300
360
CENTRAL MERIDIAN LONGITUDE
(DEGREES)
OCCURRENCE PROBABILITY
100 %
75 %
50 %
25 %
0 %

Fig. 2

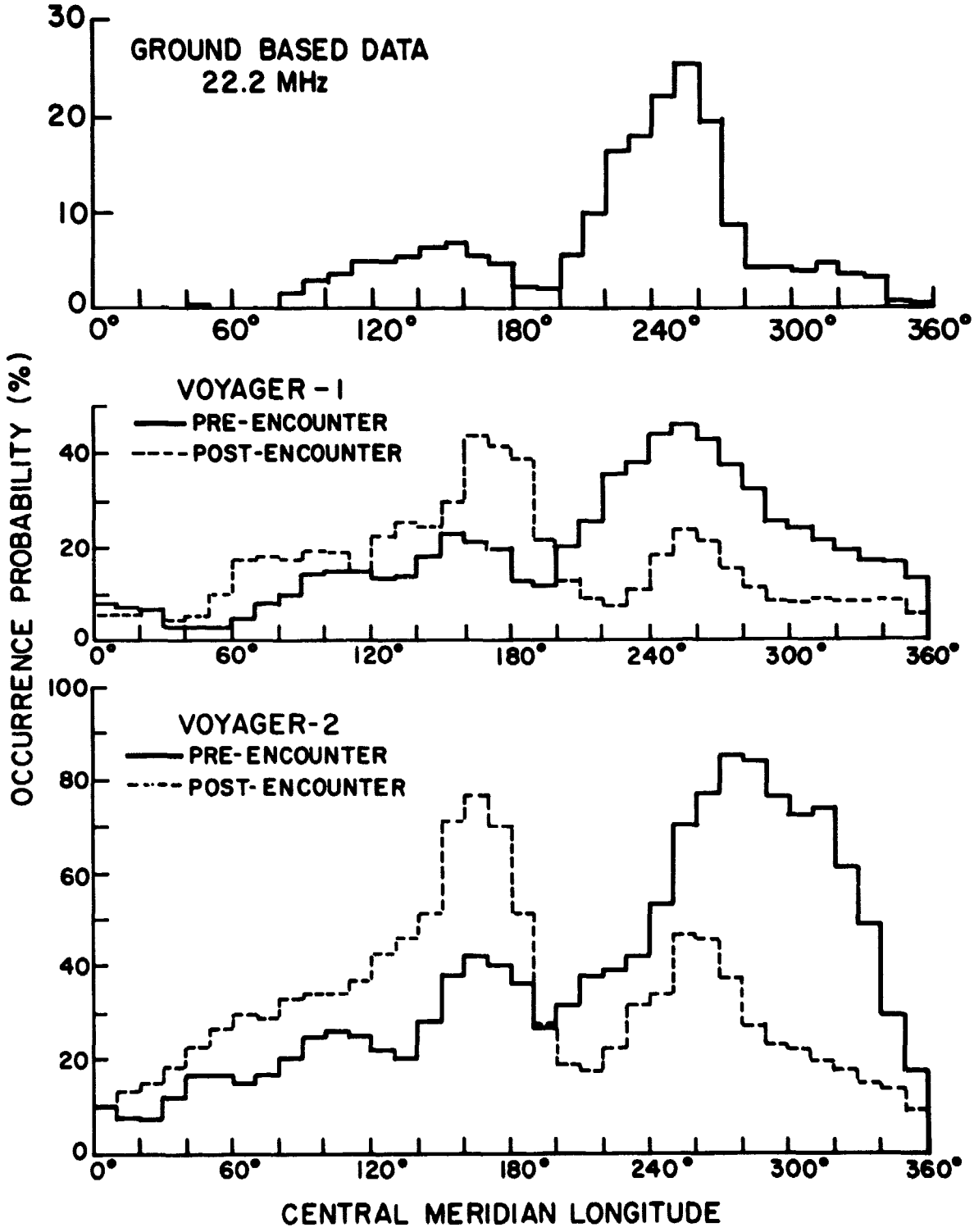
GROUND BASED DATA
22.2 MHz
VOYAGER - 1
PRE-ENCOUNTER
POST-ENCOUNTER
VOYAGER-2
PRE-ENCOUNTER
POST-ENCOUNTER
OCCURRENCE PROBABILITY (%)
CENTRAL MERIDIAN LONGITUDE
0°
60°
120°
180°
240°
300°
360°

Fig. 3

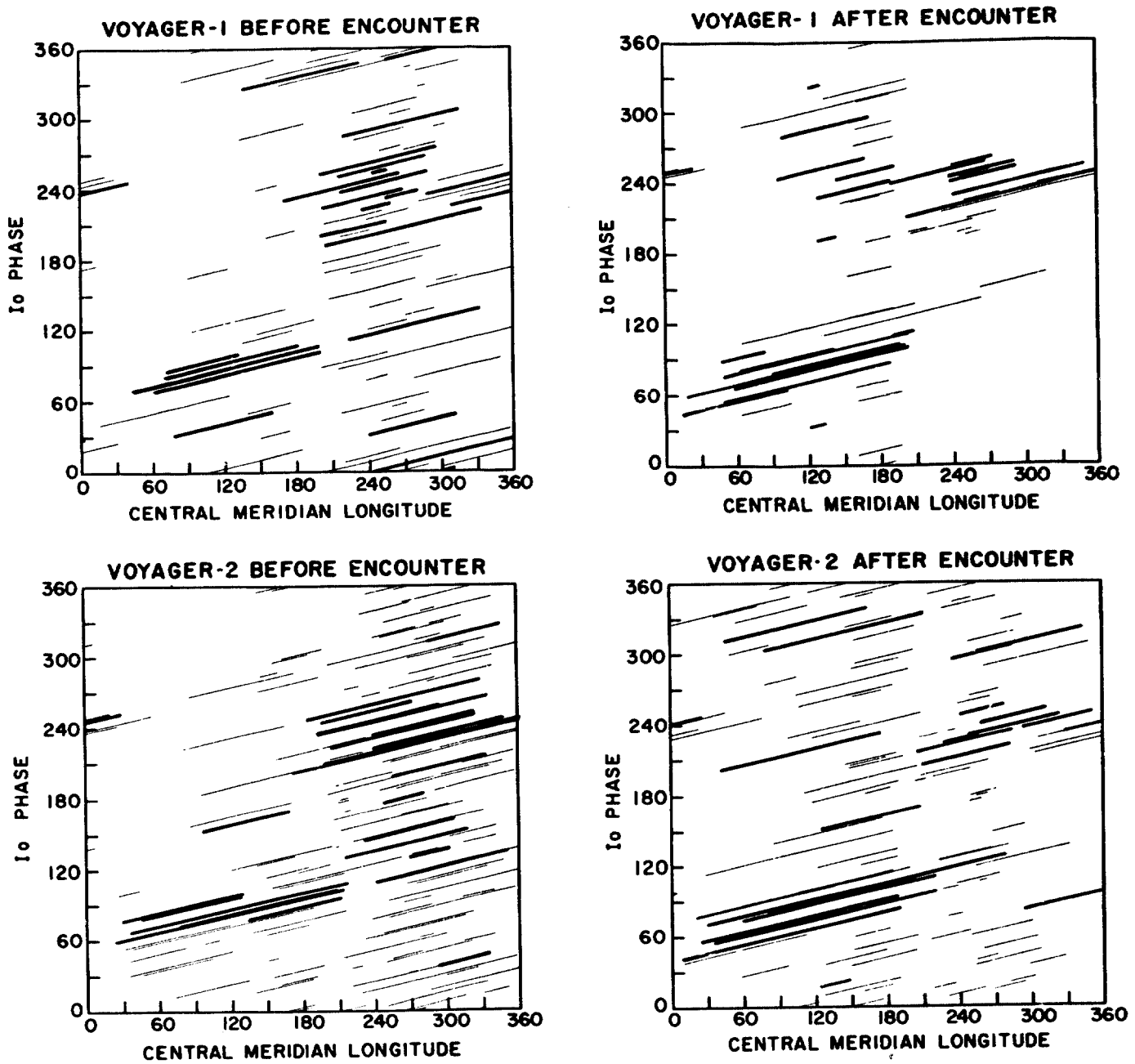
VOYAGER-1 BEFORE ENCOUNTER
VOYAGER-1 AFTER ENCOUNTER
VOYAGER-2 BEFORE ENCOUNTER
VOYAGER-2 AFTER ENCOUNTER
Io PHASE
CENTRAL MERIDIAN LONGITUDE
0
60
120
180
240
300
360

Fig. 4

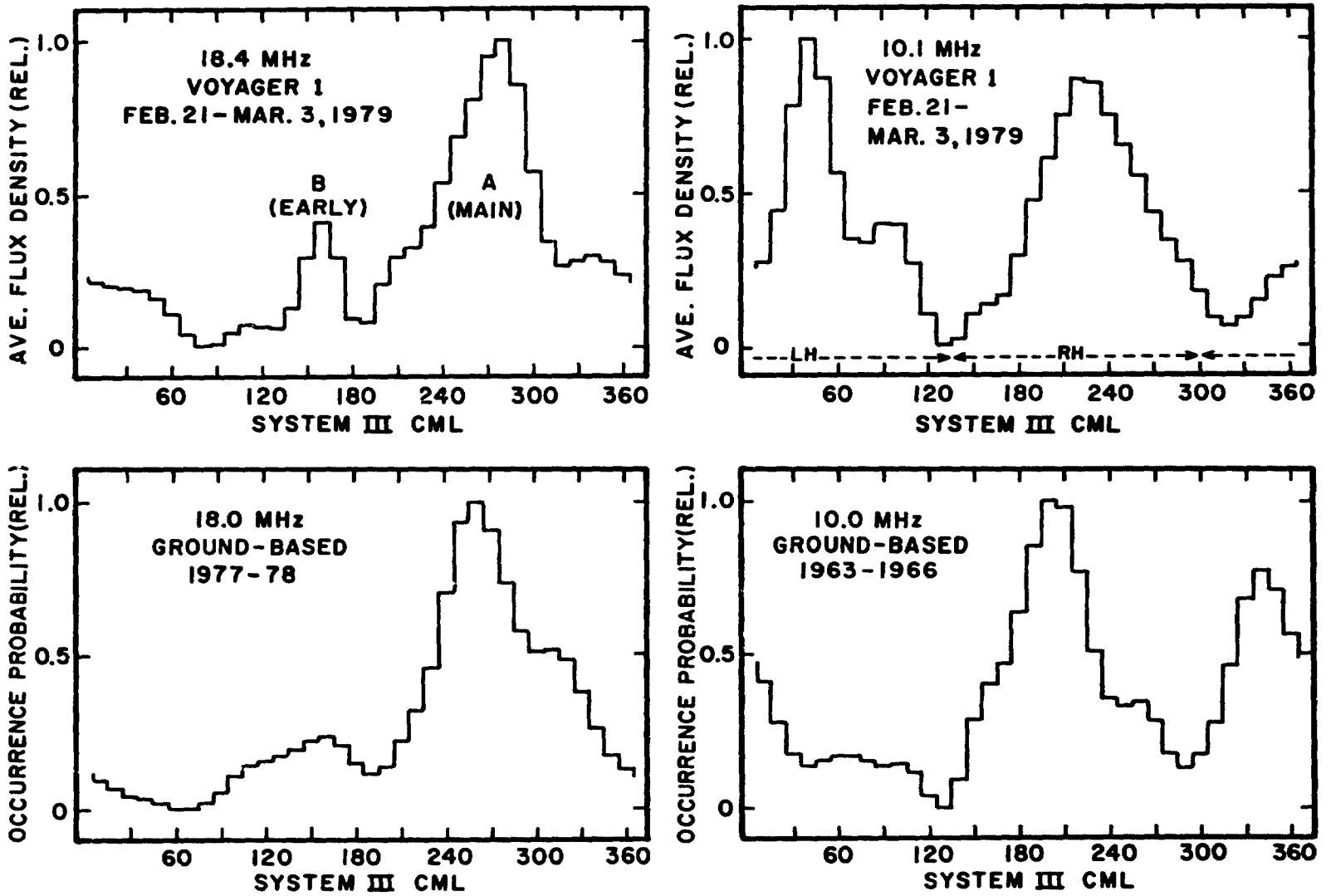
18.4 MHz
VOYAGER 1
FEB. 21 - MAR. 3, 1979
B
(EARLY)
A
(MAIN)
AVE. FLUX DENSITY (REL.)
1.0
0.5
0
60
120
180
240
300
360
SYSTEM III CML
10.1 MHz
VOYAGER 1
FEB. 21 -
MAR. 3, 1979
LH
RH
18.0 MHz
GROUND-BASED
1977-78
OCCURRENCE PROBABILITY (REL.)
10.0 MHz
GROUND-BASED
1963-1966

Fig. 5

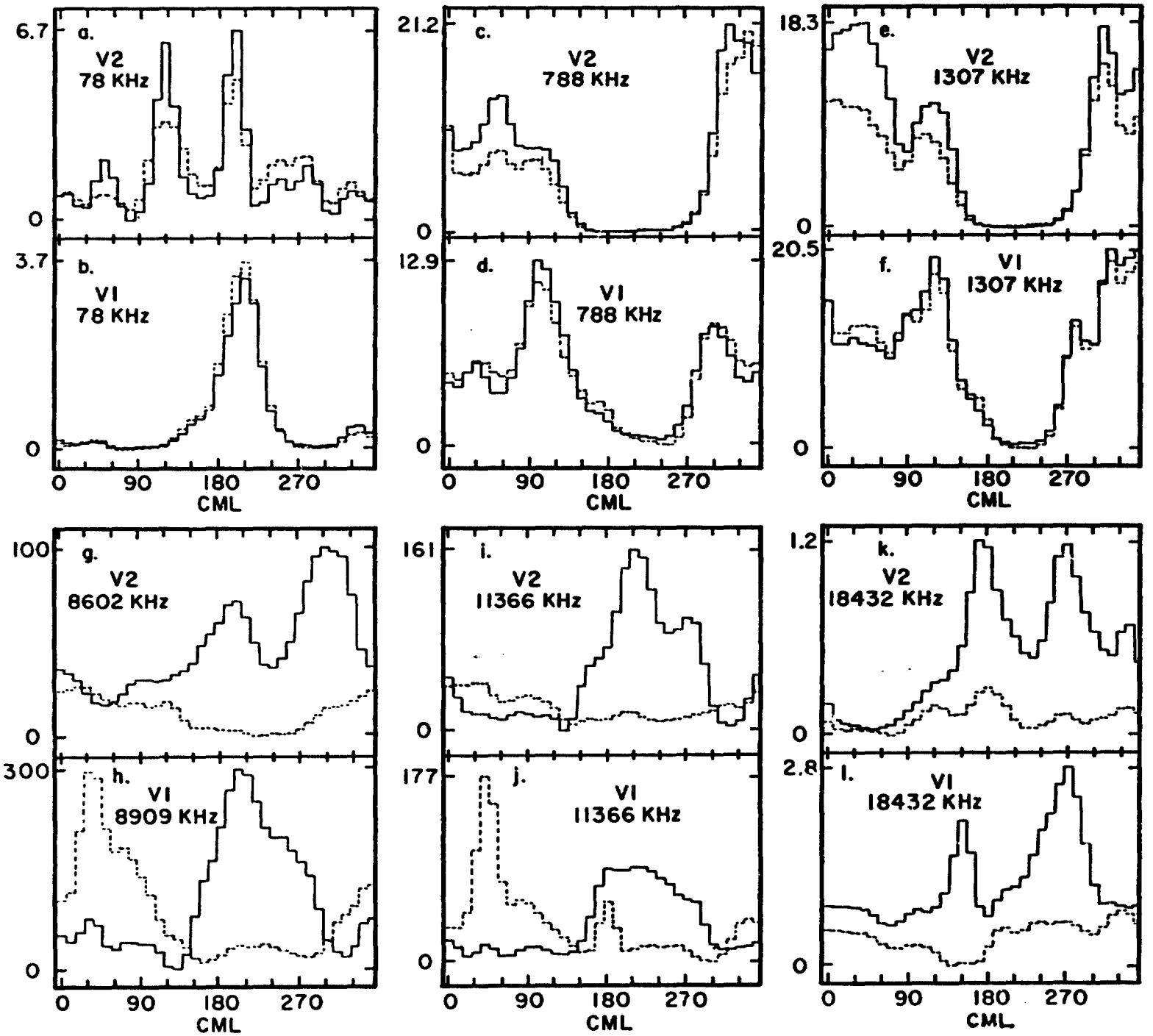
6.7
a.
V2
78 KHz
0
3.7
b.
V1
78 KHz
0
0 90 180 270
CML
21.2
c.
V2
788 KHz
0
12.9
d.
V1
788 KHz
0
0 90 180 270
CML
18.3
e.
V2
1307 KHz
0
20.5
f.
V1
1307 KHz
0
0 90 180 270
CML
100
g.
V2
8602 KHz
0
300
h.
V1
8909 KHz
0
0 90 180 270
CML
161
i.
V2
11366 KHz
0
177
j.
V1
11366 KHz
0
0 90 180 270
CML
1.2
k.
V2
18432 KHz
0
2.8
l.
V1
18432 KHz
0
0 90 180 270
CML

Fig. 6

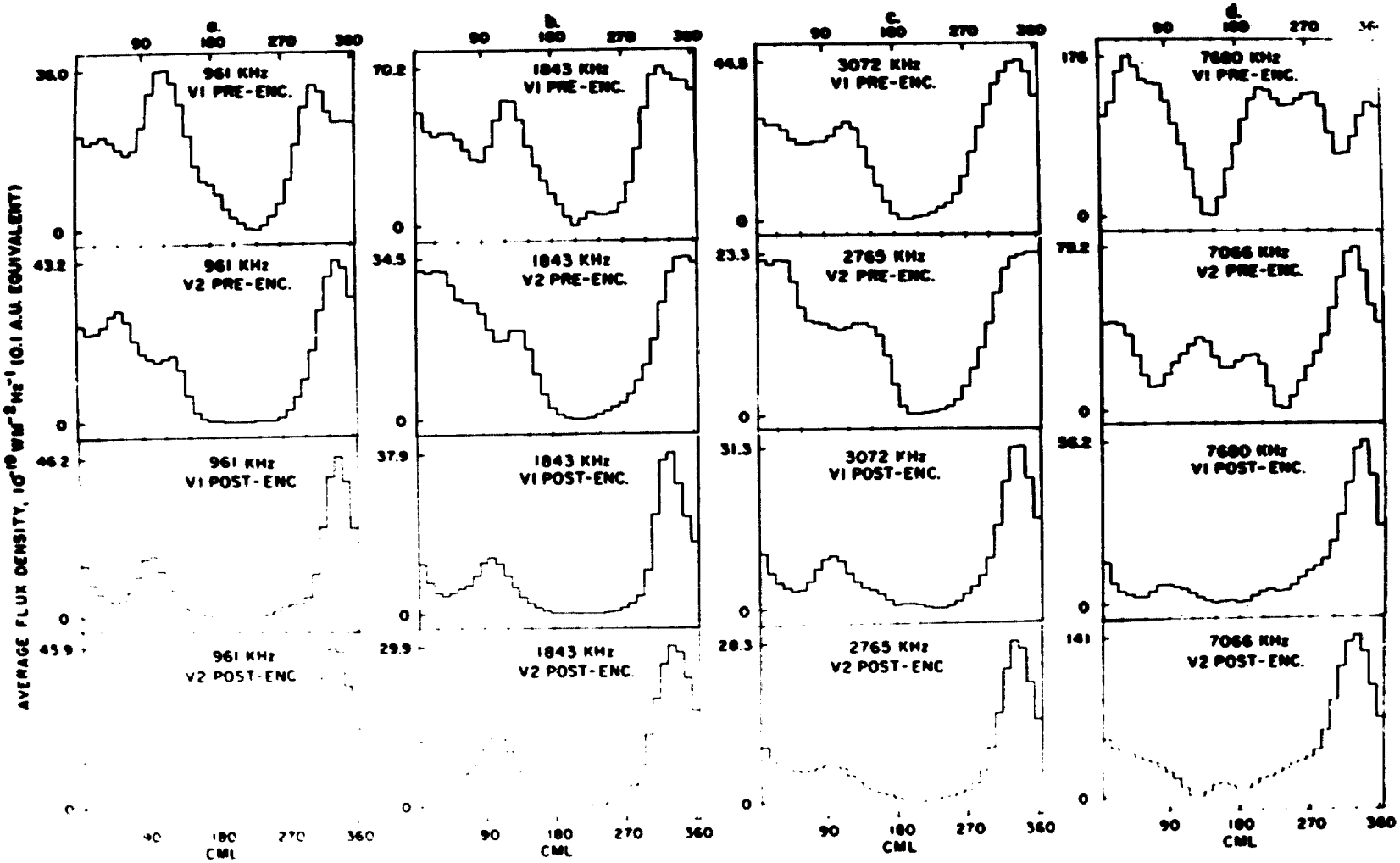
a.
b.
c.
d.
90
180
270
360
961 KHz
V1 PRE-ENC.
961 KHz
V2 PRE-ENC.
961 KHz
V1 POST-ENC
961 KHz
V2 POST-ENC
1843 KHz
V1 PRE-ENC.
1843 KHz
V2 PRE-ENC.
1843 KHz
V1 POST-ENC.
1843 KHz
V2 POST-ENC.
3072 KHz
V1 PRE-ENC.
2765 KHz
V2 PRE-ENC.
3072 KHz
V1 POST-ENC.
2765 KHz
V2 POST-ENC
7680 KHz
V1 PRE-ENC.
7066 KHz
V2 PRE-ENC.
7680 KHz
V1 POST-ENC.
7066 KHz
V2 POST-ENC.
CML
AVERAGE FLUX DENSITY, 10^{-19} WM^{-2}Hz^{-1} (0.1 A.U. EQUIVALENT)

Fig. 7

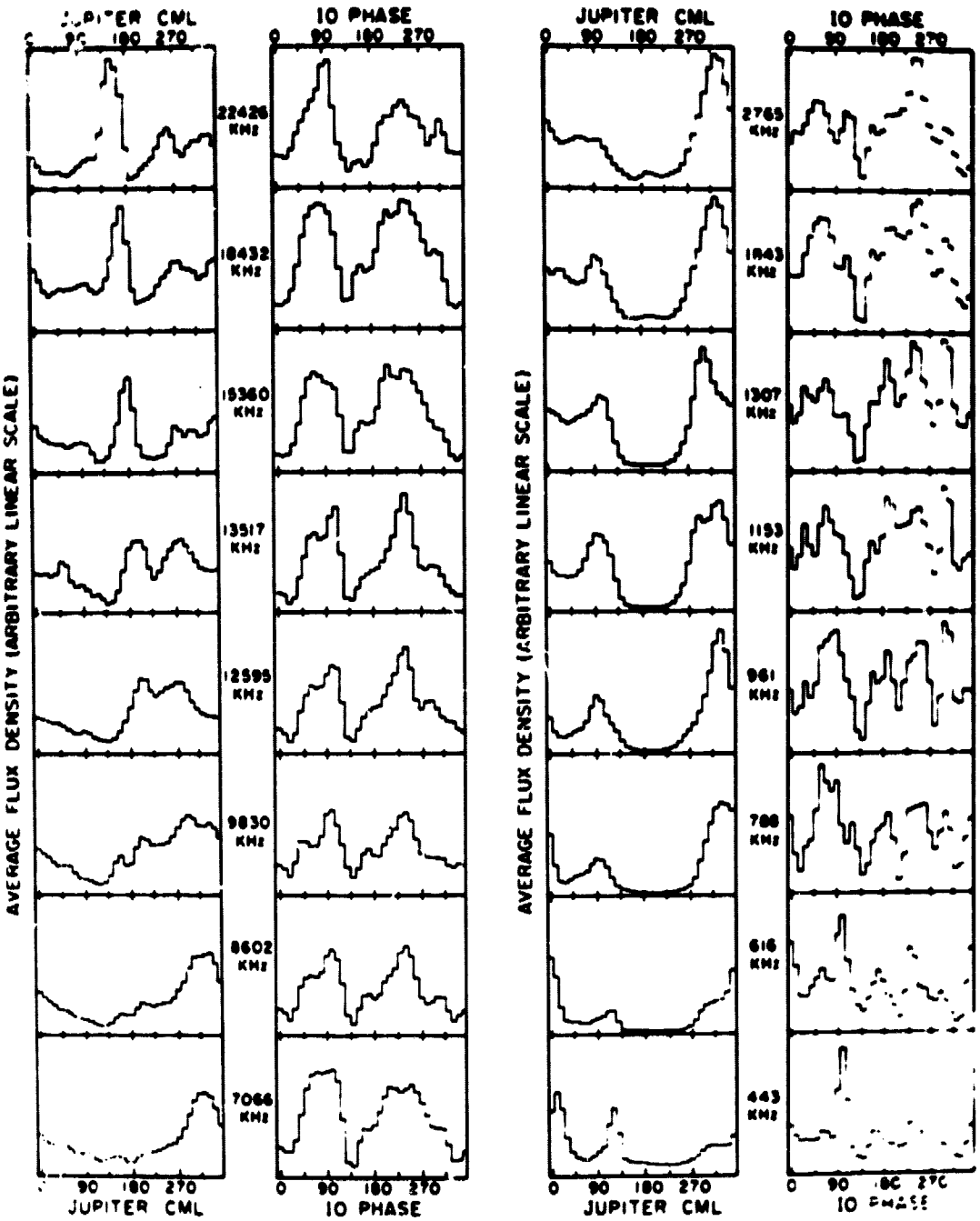
JUPITER CML
IO PHASE
JUPITER CML
IO PHASE
AVERAGE FLUX DENSITY (ARBITRARY LINEAR SCALE)
AVERAGE FLUX DENSITY (ARBITRARY LINEAR SCALE)
22425 KHz
18432 KHz
15360 KHz
13517 KHz
12599 KHz
9830 KHz
8602 KHz
7066 KHz
2765 KHz
1843 KHz
1307 KHz
1153 KHz
961 KHz
768 KHz
616 KHz
443 KHz
0 90 180 270
JUPITER CML
IO PHASE
JUPITER CML

Fig. 8

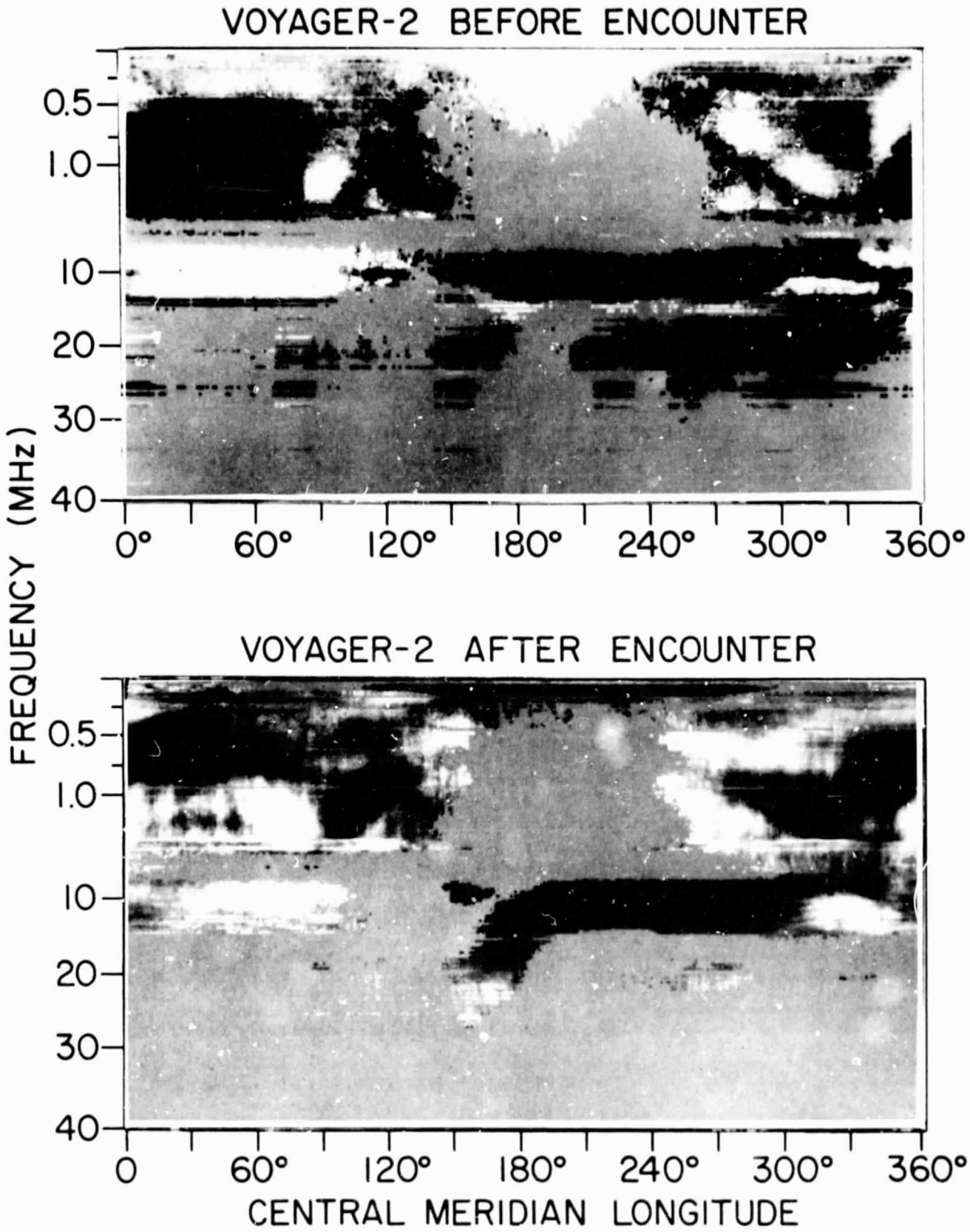

Fig. 9

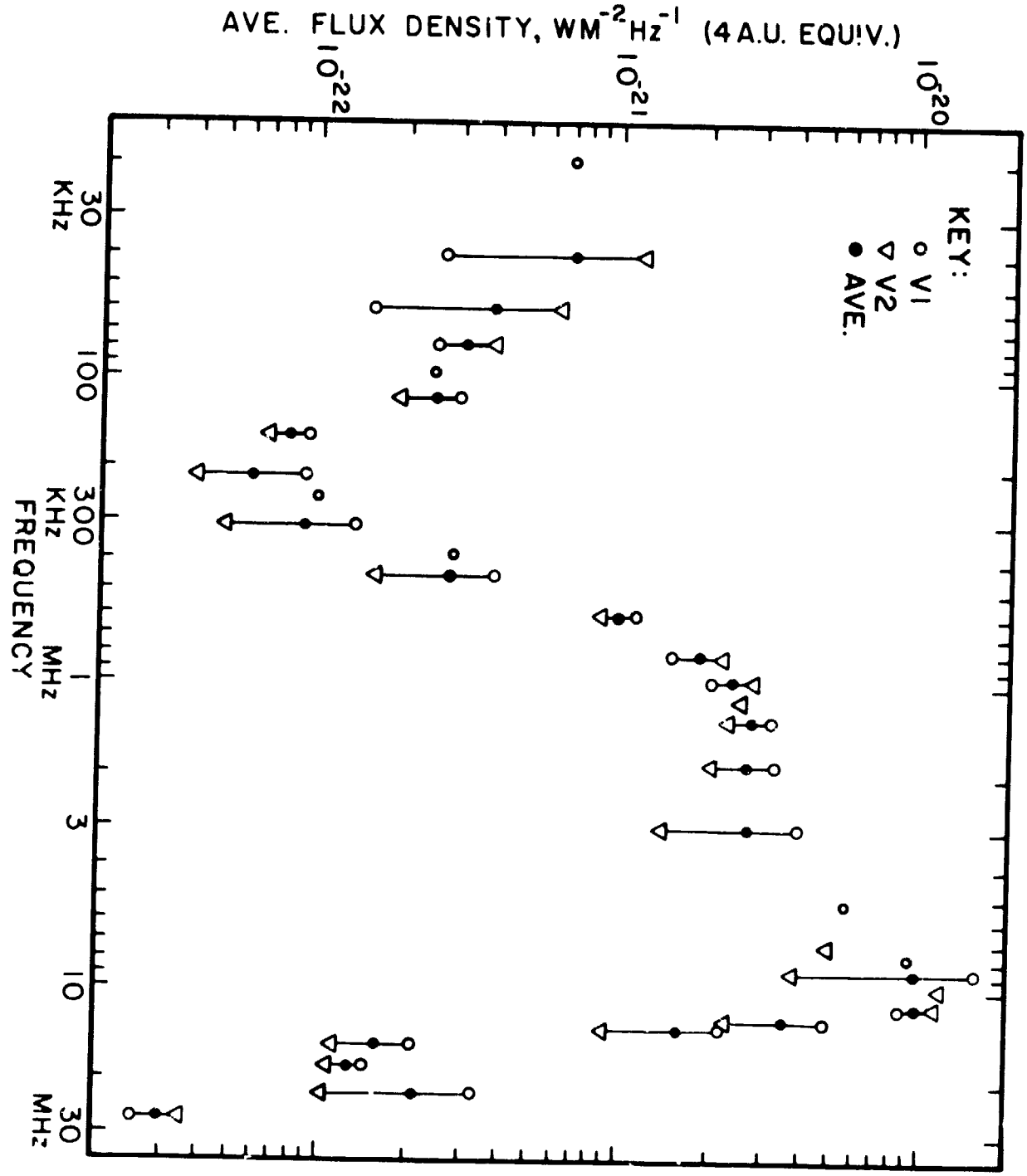
AVE. FLUX DENSITY, WM^{-2}Hz^{-1} (4 A.U. EQUIV.)
10^{-22}
10^{-21}
10^{-20}
KEY:
V1
V2
AVE.
30 KHz
100
300 KHz
1 MHz
3
10
30 MHz
FREQUENCY

Fig. 10

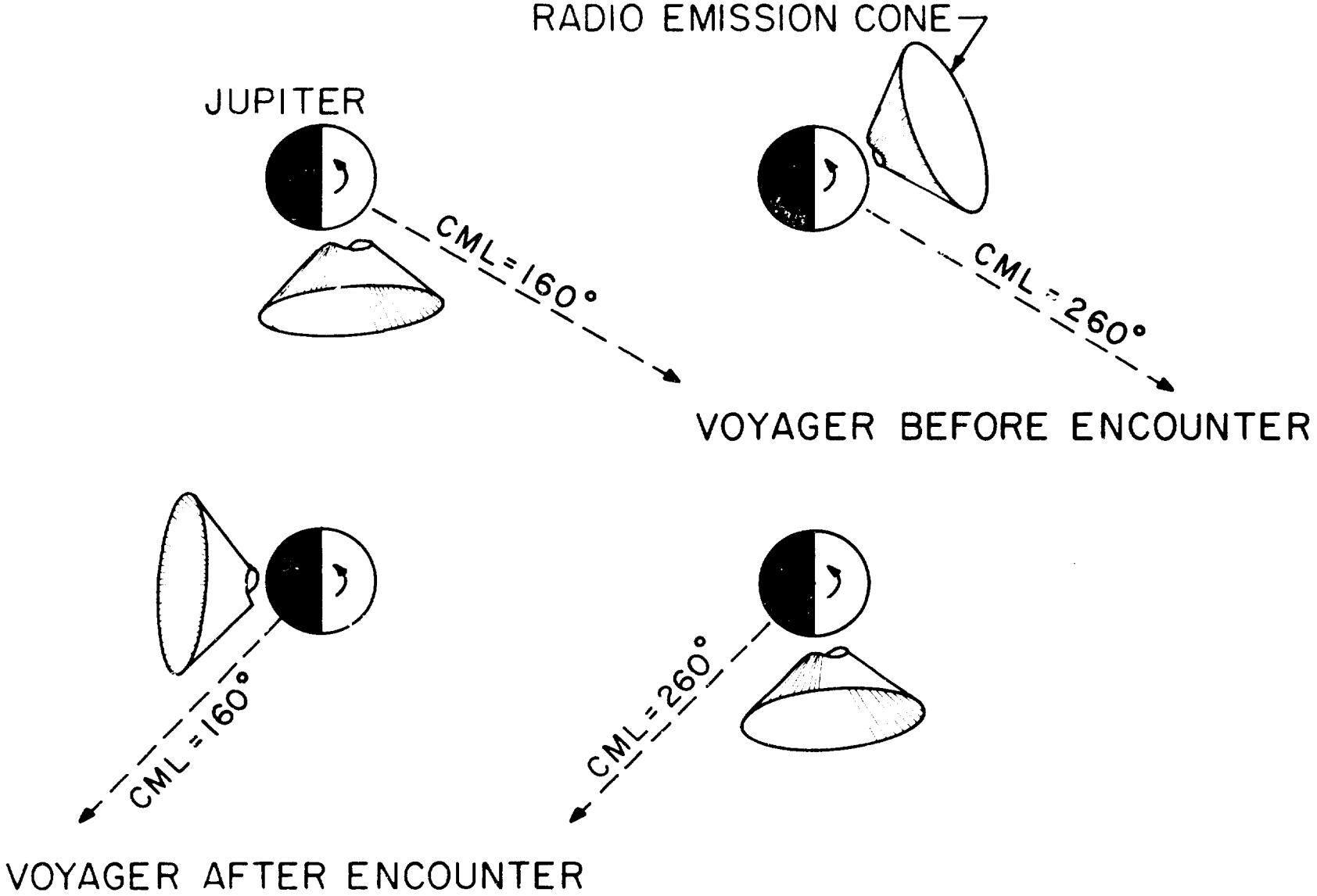
RADIO EMISSION CONE
JUPITER
CML=160°
CML=260°
VOYAGER BEFORE ENCOUNTER
CML=160°
CML=260°
VOYAGER AFTER ENCOUNTER

Fig. 11